JOURNAL OF PROPULSION AND POWER
Vol. 19, No. 4, July–August 2003

# System Performance and Thermodynamic Cycle Analysis of Airbreathing Pulse Detonation Engines

Yuhui Wu,* Fuhua Ma,† and Vigor Yang‡
*Pennsylvania State University, University Park, Pennsylvania 16802*

**A modular approach to the study of system performance and thermodynamic cycle efficiency of airbreathing pulse detonation engines (PDEs) is described. Each module represents a specific component of the engine, and its dynamic behavior is formulated using conservation laws in either one or two spatial dimensions. A framework is established for assessing quantitatively the influence of all known processes on engine dynamics. Various loss mechanisms limiting the PDE performance are identified. As a specific example, a supersonic PDE for high-altitude applications is studied comprehensively. The effects of chamber configuration and operating sequence on the engine propulsive efficiency are examined. The results demonstrate the existence of an optimum cycle frequency and valve close-up time for achieving maximum performance in terms of thrust and specific impulse. Furthermore, a choked convergent–divergent nozzle is required to render the PDE competitive with other airbreathing propulsion systems, such as gas-turbine and ramjet engines.**

## Nomenclature

| | | |
|---|---|---|
| $A$ | = | cross-sectional area of detonation tube |
| $C_p$ | = | constant-pressure specific heat |
| $D$ | = | diameter of detonation tube |
| $D_e$ | = | diameter of nozzle exit |
| $D_t$ | = | diameter of nozzle throat |
| $F$ | = | thrust |
| $F_{\text{sp}}$ | = | specific thrust (air-based), $F/\dot{m}_a$ |
| $f$ | = | ratio of fuel to air mass flow rate |
| $g$ | = | gravitational acceleration |
| $h$ | = | flight altitude |
| $I$ | = | impulse |
| $I_{\text{sp}}$ | = | specific impulse (fuel-based), $F/(\dot{m}_f g)$ |
| $L$ | = | length of detonation tube |
| $L_{\text{nozzle}}$ | = | length of nozzle section |
| $M$ | = | Mach number |
| $MR$ | = | molar ratio of nitrogen to oxygen |
| $\dot{m}$ | = | mass flow rate |
| $p$ | = | pressure |
| $p_p$ | = | plateau pressure in single-pulse detonation study |
| $q$ | = | heat addition per unit mass of air |
| $\tilde{q}$ | = | nondimensional heat addition, $q/C_{p1}T_0$ |
| $s$ | = | entropy |
| $T$ | = | temperature |
| $u$ | = | velocity |
| $\alpha$ | = | half conical angle of nozzle |
| $\beta$ | = | ratio of nozzle length to detonation tube length |
| $\gamma$ | = | ratio of specific heat |
| $\eta_{\text{th}}$ | = | thermodynamic cycle efficiency |
| $\tau$ | = | time period |
| $\tau_D$ | = | residence time of detonation wave, $L/u_D$ |
| $\phi$ | = | stoichiometric ratio |
| $\psi$ | = | cycle static-temperature ratio, $T_1/T_0$ |

*Subscripts*

| | | |
|---|---|---|
| $a$ | = | air |
| close | = | time duration during which valve is closed |
| cycle | = | pulse detonation engine operation cycle |
| $D$ | = | detonation wave |
| $f$ | = | fuel |
| $i$ | = | preconditioned state |
| purge | = | purging stage |
| refill | = | refilling stage |
| 0 | = | freestream condition |
| 1 | = | fresh reactant upstream of detonation wave front |
| 2 | = | combustion product downstream of detonation wave front |
| 3 | = | flow property after isentropic expansion |

## I. Introduction

PULSE detonation engines (PDEs) have recently been recognized as a promising propulsion technology that offers advantages in thermodynamic cycle efficiency, hardware simplicity, operation scalability, and reliability.[1] The potential for self-aspirating operation is highly attractive from the perspectives of efficiency and operation. Studies of PDEs have been conducted for several decades. The earliest experimental investigation may be traced back to Hoffman.[2] Nicholls et al.[3] later performed a series of single-pulse detonation experiments with hydrogen/oxygen and acetylene/oxygen mixtures. Because a low-energy spark ignitor was used in their experiments and no deflagration-to-detonation (DDT) augmentation device was utilized, it is not clear whether full detonation waves were realized. Significant progress was made by Krzycki[4] at the U.S. Naval Ordinance Test Station, demonstrating the use of propane/air mixtures for a pulse detonation device. The tube had an internal diameter of 1 in. (2.54 cm) and a length of 6 ft. (182.9 cm). Cycle frequency of up to 55 Hz was achieved using a high-energy spark discharge. Krzycki concluded that this intermittent detonation device was not promising for propulsion applications due to the low specific impulse associated with the limited cycle rates attained.

Exploratory research on detonation as an alternative reaction mechanism for airbreathing and rocket propulsion was terminated in the late 1960s due to the lack of funding and was not resumed until the 1980s. Helman et al.[5] carried out a series of experiments with ethylene/oxygen and ethylene/air mixtures at the U.S. Naval Postgraduate School. Both single- and multicycle modes were studied. A predetonator using ethylene/oxygen was employed to enhance the DDT process in the main tube filled with an ethylene/air mixture. The pressure recordings, however, suggested that full detonation

Received 23 October 2002; revision received 7 March 2003; accepted for publication 7 March 2003. 

*Postdoctoral research associate, Department of Mechanical Engineering; yxw119@psu.edu.

†Ph.D. Candidate, Department of Mechanical Engineering; mafuhua@psu.edu.

‡Distinguished Professor, Department of Mechanical Engineering; vigor@psu.edu. Fellow AIAA.

**Table 1 Survey of single-pulse, single-tube experimental investigations of PDEs**

| Propellant | Reference | Configurations | $I_{sp}$, s, impulse |
|---|---|---|---|
| $H_2/O_2$, 1 atm, 298 K, $\phi = 1.0$ | Hinkey et al.[6] (1995) | $L$ = unknown, i.d. = 5.1 cm, fully filled, spark ignitor of 1.7 J, DDT enhanced by Shchelkin spiral | Mixture-based, 240 s,[a] 185 s[b] |
| | Sterling et al.[7] (1996) | $L$ = 175.9 cm, i.d. = 2.2 cm, fully filled, spark ignitor | N/A |
| | Litchford[8] (2001) | $L$ = 90 cm, i.d. = 5 cm, partially and fully filled, $\phi$ unknown, spark plug of 0.11 J, DDT enhanced by Shchelkin spiral | Peak thrust = 1201 N (in fully filled case) |
| | Shepherd et al.[9] (2002) | $L$ = 800 cm, i.d. = 28 cm, fully filled, diluted with Ar or $N_2$, predetonator (direct initiation using exploding wire) | N/A |
| $H_2$/air, 1 atm, 298 K, $\phi = 1.0$ | Hinkey et al.[6] (1995) | $L$ = unknown, i.d. = 5.1 cm, fully filled, spark ignitor of 1.7 J, DDT enhanced by Shchelkin spiral, predetonator filled with $H_2/O_2$ mixtures | Fuel-based, 1000 s[a] 1200 s[b] |
| | Meyer et al.[10] (2002) | $L$ = 91.4 cm, i.d. = 5.1 cm, spark ignitor with DDT enhanced by Shchelkin spiral, extended cavity plus Shchelkin spiral, and coannulus. | N/A |
| $C_2H_4/O_2$, 1 atm, 298 K, $\phi = 1.0$ | Sanders et al.[11] (2000) | $L$ = 135 cm, i.d. = 3.8 cm, partially and fully filled, spark ignitor | Total impulse = 3000 N · s/m$^2$,[a] 792 s |
| | Daniau et al.[12] (2000) | Exploding wire source of 30 J, i.d. = 5.0 cm, $L$ = 6.5 cm, no nozzle, fully filled, $L$ = 6.5 cm, straight nozzles $L$ = 10 cm, diverging nozzles | Mixture-based, 200 s[c] >200 s[c] 257–340 s[c] |
| | Sinibaldi et al.[13] (2001) | $L$ = 120 cm, i.d. = 12.7 cm, $\phi$ = 0.2–1.0, spark ignitor with DDT enhanced by Shchelkin spiral | N/A |
| | Falempin et al.[14] (2001) | $L$ = unknown, i.d. = unknown, ignition source unknown | Mixture-based, 200 s |
| $C_2H_4$/air, 1 atm, 298 K | Broda et al.[15] (1999) | $L$ = 182.9 cm, i.d. = 3.4 cm, $\phi$ = 1.1–1.3, fully filled, spark ignitor of 3.5 J, DDT enhanced by obstacles | N/A |
| | Sanders et al.[11] (2000) | $L$ = 135 cm, i.d. = 3.8 cm, $\phi$ = 1.3, fully filled, spark ignitor with DDT enhanced by Shchelkin spiral | N/A |
| | Watts et al.[16] (2000) | Square tube, $W$ = 4.5 cm, $L$ = 165 cm, $\phi$ = 1.2, fully filled, spark plug of 25 J, DDT enhanced by obstacles | N/A |
| | Sinibaldi et al.[17] (2000) | $L$ = 120 cm, i.d. = 12.7 cm, $\phi$ = 1.0, predetonator, spark ignitor with unknown energy | N/A |
| $C_2H_4/O_2/N_2$, $p$ and $T$ unknown | Sinibaldi et al.[17] (2000) | $L$ = 190.5 cm, i.d. = 5.7 cm, $\phi$ = 0.6–2.0, fully filled, ignitor of 0.33–8.31 J, $O_2/N_2$ volumetric ratio: 100% and 75% | N/A |
| $C_2H_4/O_2/N_2$, 30–100 kPa, 298 K | Cooper et al.[18] (2002) | $L$ = 101.6 cm ($L/D$ = 13), i.d. = 7.6 cm, $\phi$ = 1.0, fully filled, spark ignitor, $N_2$ dilution: 0–75% (by volume) | Mixture-based 170 s[c] at $p$ = 100 kPa |
| $C_3H_8/O_2$, 1 atm, 298 K | Sinibaldi et al.[13] (2001) | $L$ = 120 cm, i.d. = 12.7 cm, $\phi$ = 0.4–1.0, predetonator, spark ignitor | N/A |
| | Harris, et al.[19] (2001) | $L$ = 250 cm, i.d. = 5.05 cm, $\phi$ = 1.0, fully filled, spark plug of 0.05 J for DDT initiation, exploding wire ignitor of 203–502 J for direct initiation | Total impulse = 10 N · s[c] ($MR$ = 0) 8.0 N · s[c] ($MR$ = 1.0) |
| $C_3H_8/O_2/N_2$, 0.5–1.0 atm, 298 K, $\phi = 1.0$ | Cooper et al.[18] (2002) | Tube fully filled, $N_2$ dilution: 0–75% (by volume), i.d. = 7.6 cm, $L$ = 60.9 cm ($L/D$ = 8), various spiral pitches i.d. = 3.8 cm, $L$ = 150 cm ($L/D$ = 40), spiral pitch = 1.1 cm | Mixture-based, at $p$ = 100 kPa without $N_2$ dilution: 150 s[c], 172 s[c] ($L/D$ = 8) 130 s[c] ($L/D$ = 40) |
| $C_3H_8/O_2/N_2$, 1 atm, $T$ unknown, $\phi = 1.0$ | Lieberman et al.[20] (2002) | $L$ = 100 cm, i.d. = 7.5 cm, $N_2$ dilution: 20–40% (by volume), driver section: $C_3H_8/O_2$ ($\phi$ = 1) at $p$ = 1, 4 atm $L$ = 14 cm, i.d. = 3 cm, spark plug of 30 mJ | Mixture-based, 152 s[c] (20% $N_2$ dilution) 144 s[c] (40% $N_2$ dilution) |

[a]Based on time history of pressure at thrust wall. [b]Based on time history of force measured by load cell. [c]Maximum impulse measured from ballistic pendulum displacement.

was not achieved, as revealed by the presence of significant compression waves preceding the pressure rise of the reported detonation waves.

Much effort has been applied to the study of various aspects of PDEs since the mid-1990s. Tables 1 and 2 summarize the experimental work performed to date.[6–32] In single-pulse experiments, only detonation ignition, propagation, and attenuation were investigated at preconditioned states. Total impulse was obtained based on measured chamber pressure and/or force histories for a limited time period. In practice, negative thrust may appear due to the low-energy level of the gases in detonation tubes during the blowdown, purging, and refilling processes in a multicycle mode. As a result, system performance obtained from single-pulse experiments usually exceeded that in a real engine with multicycle operation. In contrast, multicycle experiments involved all necessary PDE operation processes and, thus, provided more direct simulation. However, much important information required to characterize the system dynamics, such as airflow rate and purging/refilling data, was not measured in most experiments. The details for thrust measurements were not clearly defined either, rendering assessment of the performance of different systems a difficult task.

In parallel to experimental investigations, attempts were made both theoretically and numerically to estimate the performance of PDEs. Talley and Coy[33] employed a lumped-parameter analysis to determine the theoretical limit of PDE performance by approximating detonation chamber dynamics with an ideal constant-volume process. The blowdown time was assumed to be much longer than the characteristic wave transit times in the chamber. Tew[34] and Kentfield[35] estimated the PDE performance using an ideal-cycle assumption. Detonation was approximated as either a polytropic or a constant-volume heat addition process. Heiser and Pratt[36] utilized a more realistic Zeldovich, von Neumann, and Döring (ZND) model to simulate the detonation process in their PDE cycle analysis. Wintenberger et al.[37] developed a semi-analytical model for the impulse of a single-pulse detonation tube by means of dimensional analysis and empirical observations. In addition to these theoretical models, several numerical analyses based on one-dimensional[38,39] and two-dimensional[40–47] approaches were carried out. One major deficiency of one-dimensional analyses is that the boundary condition at the detonation tube exit can not be correctly specified because it depends on the local flow evolution in the downstream ambient regime.[46] Multidimensional simulations with computational

**Table 2 Survey of multicycle experimental investigation of PDEs**

| Propellants | Reference | Configurations | $I_{sp}$, s and Thrust, N |
|---|---|---|---|
| $H_2/O_2$, 1 atm, 298 K, $\phi = 1.0$ | Sterling et al.[7] (1996) | Single tube, $f = 33$ Hz, i.d. $= 2.2$ cm, $L = 15.2$ cm fully filled, $H_2$ and $O_2$ adopted as buffer gases, spark ignitor | N/A |
| | Stuessy and Wilson[21] (1996) | Single tube, $f = 10$–12 Hz, fully filled, air used as buffer gas cylindrical tube with i.d. $= 7.6$ cm, $L = 53.3$ cm annular tube with i.d. $= 2.5$ cm, o.d. $= 7.6$ cm, $L = 53.3$ cm annular tube with diverging conical nozzle | N/A |
| $H_2$/air, 1 atm, 298 K | Aarnio et al.[22] (1996) | Single tube, $f = 5$ Hz, i.d. $= 5.1$ cm, $L = 121.9$ cm, $\phi = 1.0$ partially filled, air used as buffer gas, spark ignitor of 1.7 J | Fuel-based, 1333 s[a] 1116 s[b] |
| | Hinkey et al.[23] (1997) | Twin tube, $f = 10$ Hz, common air inlet manifold, i.d. $= 5.1$ cm, $L = 91.4$ cm, $\phi = 0.7$–1.3 predetonator filled by $H_2/O_2$ mixtures, spark ignitor of 1.5 J | N/A |
| | Schauer et al.[24] (1999) | Multitube (1, 2, and 4), $f = 0.5$–100 Hz, i.d. $= 5.1$ cm, $L = 91.4$ cm and i.d. $= 8.9$ cm, $L = 91.4$ cm, air used as buffer gas, spark ignitor with DDT enhanced by Shchelkin spiral | N/A |
| | Schauer et al.[25] (2000) | $f = 14$–40 Hz, $L = 91.4$ cm, i.d. $= 5.1$ cm, $\phi = 0.4$–2.85 spark ignitor with DDT enhanced by Shchelkin spiral, air used as buffer gas with 50% tube filling ratio, various ignition delays and tube filling fractions | Fuel-based for $\phi = 1.0$, $f = 16$ Hz, and 3.5 s ignition delay: 7100 s[a] (30% filling length) 4200 s[a] (90% filling length) |
| | McManus et al.[26] (2001) | Single tube, $f = 10$–35 Hz, conical converging nozzle, i.d. $= 4.76$ cm, $L = 25.4$ cm, $\phi = 0.6$, spark ignitor of 0.02 J at tube exit | $F = 11.12$ N[b] ($f = 10$ Hz) $F = 53.38$ N[b] ($f = 35$ Hz) |
| | Frankey et al.[27] (2002) | Single tube, $f = 11$–21 Hz, converging nozzle, i.d. $= 5.08$ cm, $L = 182.88$ cm, $\phi = 1.0$, spark ignitor with DDT enhanced by Shchelkin spiral, air used as buffer gas | $F = 222$ N[a] ($f = 21$ Hz) |
| $C_2H_4/O_2$, 1 atm, 298 K, $\phi = 1.0$ | Sterling et al.[7] (1996) | $f = 100$ Hz, $L = 50.8$ cm, i.d. $= 2.2$ cm, 1/3 tube filled, spark ignitor with DDT enhanced by unspecified device | N/A |
| | Falempin et al.[14] (2001) | Single tube, $f = 80$ Hz, i.d. $= 5.0$ cm, $L = 5.0$–42.6 cm, ignition source not mentioned | N/A |
| $C_2H_4$/air, 1 atm, 298 K | Broda et al.[15] (1999) | $f = 8$–10 Hz, $L = 182.9$ cm, i.d. $= 3.4$ cm, $\phi = 1.1$, spark ignitor of 4–8 J, DDT enhanced by obstacles | N/A |
| | Watts et al.[16] (2000) | Single tube, $f = 10$ Hz, $\phi = 1.2$, spark plug of 25 J, DDT enhanced by obstacles, buffer air injected for 5–10 ms in each cycle | N/A |
| | Brophy et al.[28] (2002) | Single tube, $f = 80$ Hz, i.d. $= 4.0$ cm, $L = 25$ cm, $\phi = 1.0$–1.8, spark ignitor with unknown energy | Total impulse, 0.48 N · s[a] ($\phi = 1.0$) |
| | Shimo et al.[29] (2002) | $f = 15$ Hz, i.d. $= 5.1$ cm, $L = 82.2$ cm, $\phi = 0.9$, 60% filling ratio, spark ignitor with DDT enhanced by Shchelkin spirals | N/A |
| JP-10/$O_2$ g $p$ and $T$ unknown | Brophy et al.[30] (1998) | $f = 5$ Hz, $L = 15.2$, 30.5, 76.2 cm, i.d. $= 3.8$ cm, $\phi = 0.7$–1.7, ignitor of 1.4 J, ignition delay: 40, 50, and 70 ms | N/A |
| 1 atm, 292 K | Brophy and Netzer[31] (1999) | Single tube, $f = 10$ Hz, i.d. $= 3.81$ cm, $L = 29$ cm, $\phi = 0.9$–1.2, ignitor of 0.5 J at locations $x = 0$–2D from head end | N/A |
| 1 atm, 280 K | Brophy et al.[28] (2002) | Single tube, $f = 30$ Hz, i.d. $= 4.0$ cm, $L = 25$ cm, $\phi = 1.0$–1.8, spark ignitor with unknown energy | Total impulse, 0.59 N · s[a] ($\phi = 1.0$) |
| $C_3H_8/O_2$, $p$ and $T$ unknown | Farinaccio et al.[32] (2002) | $f = 10$, 15, 20, 25 Hz, $L = 40$ cm, i.d. $= 8.1$ cm, $\phi = 1.0$, fully or partially filled, $N_2$ purged for 1/3-cycle period | Mixture-based, 71 s[b] ($f = 15$ Hz) 71 s[b] ($f = 20$ Hz, fully filled) |

[a]Based on time history of pressure at thrust wall. [b]Based on time history of force measured by load cell.

domains including both detonation tubes and ambient flows are, thus, required to describe the system dynamics faithfully, especially in the near field of the tube exit, where the flow is intrinsically multidimensional. To date, only single-pulse operations have been treated using two-dimensional analyses. Multicycle simulations have been limited to one-dimensional models, whose results are apparently questionable. Most of the analyses developed so far have considered only detonation chamber dynamics, not a complete PDE system.

The current work attempts to establish a global analysis to determine the overall system performance and thermodynamic cycle efficiency of airbreathing PDEs. Figure 1 shows schematically the configuration under consideration. It includes a coaxial supersonic inlet with mixed compression, a multitube detonation chamber, and a nozzle. A rotary valve is placed in front of the combustor entrance to distribute the airflow evenly into the individual tubes. The following section describes the development of an ideal PDE thermodynamic cycle analysis to assess the theoretical limit of system performance. A modular approach is then utilized to analyze the engine dynamics numerically. As a specific example, an engine operating at a flight altitude of 9.3 km and a freestream Mach number of 2.1 is considered. The effects of various operating parameters on the engine propulsion efficiency are studied systematically. Finally, the influence of nozzle design is examined.

## II. Thermodynamic Cycle Analysis

An ideal thermodynamic cycle analysis is presented in this section to estimate the theoretical limit of the performance of an airbreathing PDE. The work extends the approach of Heiser and Pratt[36] for perfect gases with constant properties to accommodate property variations across the detonation wave front. Figure 2 shows the temperature–entropy diagram of an ideal PDE cycle. The corresponding Humphrey (constant-volume combustion) and Brayton (constant-pressure combustion) cycles are included for comparison. The process from point 0 to point 1 is an adiabatic, isentropic compression process, in the course of which the flow temperature is raised from its freestream value, $T_0$, to that at the combustor entrance, $T_1$. The path from point 1 to point 2 corresponds to the detonation process. Here the ZND model is adopted, that is, the dashed line from point 1 to point 1a corresponds to the entropy increase caused by shock compression and the solid line from point 1a to point 2 represents subsequent heat release due to chemical reactions. Point 2

**Table 3 Variations of flow properties for stoichiometric $H_2$/air mixture[a]**

| Cycle | $p_{1a}/p_1$ | $p_2/p_1$ | $T_{1a}/T_1$ | $T_2/T_1$ | $s_{1a}-s_1$, kJ/kg·K | $s_2-s_1$, kJ/kg·K | $\gamma_2$ |
|---|---|---|---|---|---|---|---|
| Ideal PDE | | 15.50 | 5.47 | 9.82 | 1.04 | 1.84 | 1.16 |
| Humphrey | N/A | 7.96 | N/A | 9.17 | N/A | 1.89 | 1.17 |
| Brayton | N/A | 1.00 | N/A | 7.94 | N/A | 2.28 | 1.18 |

[a] $T_1 = 300$ K, $p_1 = 1$ atm, and $\gamma_1 = 1.4$.

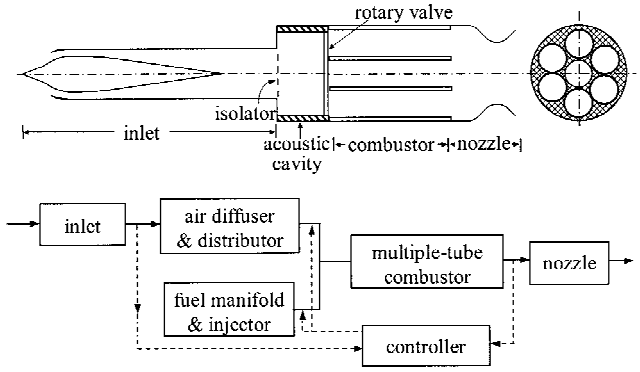


**Fig. 1 Supersonic airbreathing PDE.**

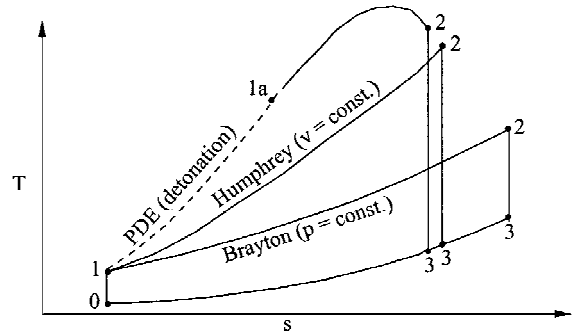


**Fig. 2 Temperature–entropy diagram of ideal PDE, Humphrey, and Brayton cycles.**

is known as the Chapman–Jouguet (C–J) point, where the chemical system reaches an equilibrium state and the flow relative to the detonation wave front is sonic. For a given initial condition and reactant composition, the detonation wave velocity and C–J properties can be easily determined by means of a chemical equilibrium analysis.[48] Table 3 summarizes the flow properties at various stations for a stoichiometric hydrogen/air mixture initially at 1 atm and 300 K. Note that the "humped" nature of the heat addition process from point 1a to point 2 reflects the well-known phenomenon of the existence of a maximum temperature when heat is added to a steady subsonic flow. The process from point 2 to point 3 involves isentropic expansion, with the pressure of the burned gases decreasing to the freestream condition $p_3 (= p_0)$. The cycle is closed by an imaginary constant static-pressure process in which the abundant heat is removed to the surroundings from the exhaust flow.

Following the conventional definition, the thermodynamic cycle efficiency $\eta_{\text{th}}$ is expressed as

$$\eta_{\text{th}} = 1 - q_{\text{reject}}/q \tag{1}$$

where $q$ and $q_{\text{reject}}$ are the amount of heat added during the process from point 1a to point 2 and the amount of heat removed to the ambient during the process from point 3 to point 0, respectively. After extending the analysis of Heiser and Pratt[36] to include property variations across the detonation wave front, a closed-form expression of $\eta_{\text{th}}$ is obtained as follows[49]:

$$\eta_{\text{th,PDE}} = 1 - \left\{ \left[ \frac{\gamma_1 - 1}{\gamma_2 - 1} \left( \frac{\gamma_2}{\gamma_1} \right)^2 \frac{1}{M_D^2} \left( \frac{1 + \gamma_1 M_D^2}{1 + \gamma_2} \right)^{(\gamma_2+1)/\gamma_2} \times \psi^{1-[(\gamma_2-1)/(\gamma_1-1)](\gamma_1/\gamma_2)} - 1 \right] \Big/ \tilde{q} \right\} \tag{2}$$

where $\gamma_1$ and $\gamma_2$ are the specific-heat ratios of the unburned and burned gases separated by the detonation wave front, respectively. The Mach number of the detonation wave relative to the unburned gas, $M_D$, can be calculated using the following equation for fixed heat addition:

$$M_D^2 = \left[ \frac{\gamma_2^2 - \gamma_1}{\gamma_1^2 - \gamma_1} + \frac{\gamma_2^2 - 1}{\gamma_1 - 1} \frac{\tilde{q}}{\psi} \right] + \sqrt{\left[ \frac{\gamma_2^2 - \gamma_1}{\gamma_1^2 - \gamma_1} + \frac{\gamma_2^2 - 1}{\gamma_1 - 1} \frac{\tilde{q}}{\psi} \right]^2 - \frac{\gamma_2^2}{\gamma_1^2}} \tag{3}$$

In comparison, the thermodynamic efficiencies of the Humphrey and Brayton cycles are

$$\eta_{\text{th,Humphrey}} = 1 - \left\{ \left[ \frac{\gamma_2}{\gamma_1} \left( \frac{\gamma_1 - 1}{\gamma_2 - 1} \right)^{(\gamma_2-1)/\gamma_2} \left( \gamma_1 \frac{\tilde{q}}{\psi} + 1 \right)^{1/\gamma_2} \times \psi^{1-[(\gamma_2-1)/(\gamma_1-1)](\gamma_1/\gamma_2)} - 1 \right] \Big/ \tilde{q} \right\} \tag{4}$$

$$\eta_{\text{th,Brayton}} = 1 - \left\{ \left[ \left( \frac{\tilde{q}}{\psi} + 1 \right) \psi^{1-[(\gamma_2-1)/(\gamma_1-1)](\gamma_1/\gamma_2)} - 1 \right] \Big/ \tilde{q} \right\} \tag{5}$$

With the thermodynamic cycle efficiency available, the thrust $F$ can be obtained by a control-volume analysis,

$$F = (\dot{m}_a + \dot{m}_f) u_3 - \dot{m}_a u_0 \approx \dot{m}_a \left( \sqrt{u_0^2 + 2\eta_{\text{th}} q} - u_0 \right) \tag{6}$$

where $u_0$ is the freestream velocity, $\dot{m}_a$ the cycle-averaged air mass flow rate delivered to the engine through the inlet, and $\dot{m}_f$ the cycle-averaged fuel mass flow rate. Note that the preceding analysis is based on the assumptions that every fluid particle experiences the same processes sequentially and that the effects of purging and bypass air are ignored. The fuel-based specific impulse can then be obtained as follows:

$$I_{\text{sp}} = \frac{F}{\dot{m}_f g} = \frac{\sqrt{u_0^2 + 2\eta_{\text{th}} q} - u_0}{fg} \tag{7}$$

Figures 3 and 4 show a typical result of cycle efficiency and specific impulse for a stoichiometric hydrogen/air system.

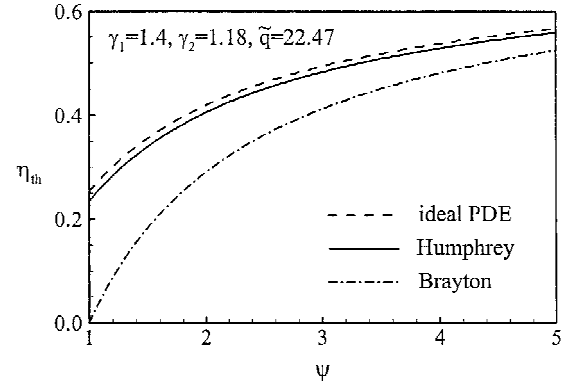


**Fig. 3 Thermodyanmic cycle efficiencies of ideal PDE, Humphrey, and Brayton cycles as function of static temperature ratio $\psi$ for stoichiometric $H_2$/air system.**

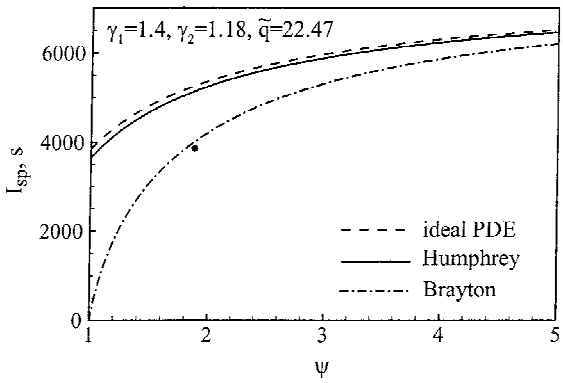


**Fig. 4 Specific impulses of ideal PDE, Humphrey, and Brayton cycles as function of static temperature ratio $\psi$ for stoichiometric $H_2$/air system.**

The freestream velocity and temperature are $u_0 = 636$ m/s and $T_0 = 228$ K, respectively. The nondimensional heat addition $q$ is 22.47. The system performance increases with increasing static temperature ratio. The PDE offers the best performance among the three cycles, especially when the static temperature ratio $\psi$ is smaller than 3. This may be because, for a given amount of heat addition, the Mach number of the detonation wave increases with decreasing $T_1$ (or $\psi$), as indicated by Eq. (3). The shock-compression effect becomes more significant for a lower $T_1$, leading to a higher increase in the temperature and pressure of the unburned gases before combustion. The $I_{sp}$ of an ideal PDE reaches 5263 s when $T_1 = 428$ K, that is, $\psi = 1.877$.

## III. System Performance Analysis

This section deals with the development of a system performance analysis for airbreathing PDEs as shown schematically in Fig. 1. The study is based on a modular approach. Each module represents a specific component of the engine, and its dynamic behavior is formulated using complete conservation equations. The work involves the following three components: 1) supersonic inlet dynamics, 2) detonation chamber dynamics and system performance, and 3) effect of nozzle configuration. The effects of fuel supply, air distribution, and inlet isolator are ignored for simplicity. They can, however, be straightforwardly included as submodels in the overall engine performance analysis.

### A. Supersonic Inlet Dynamics

The inlet and its interaction with combustor represent a crucial aspect in the development of any airbreathing engine, including PDEs. The inlet is designed to capture and supply stable airflow at a rate demanded by the combustor and to maintain high pressure recovery and stability margin at various engine operating conditions. The overall vehicle performance depends greatly on the energy level and flow quality of the incoming air. A small loss in inlet efficiency may translate to a substantial penalty in engine thrust. Moreover, any change in the inlet flow structure may modify the downstream combustion characteristics and subsequently lead to undesirable behaviors, such as flame blowoff and flashback. Thus, matching inlet behavior to engine requirements is of fundamental importance to designers.[50]

In addition to its primary function of supplying air, an inlet has a determining influence on the dynamics of the entire system through its intrinsic unsteadiness and interactions with the combustion chamber. Typically, pressure waves are produced in the combustion chamber and propagate upstream to interact with the inlet flow through a manifold, where mixing of air and fuel occurs. The resultant flow oscillations in the inlet diffuser then either propagate downstream in the form of acoustic waves, or are convected downstream with the mean flow in the form of vorticity and entropy waves, and further reinforce the unsteady motions in the combustor. A feedback loop is, thus, established between the inlet and combustor.

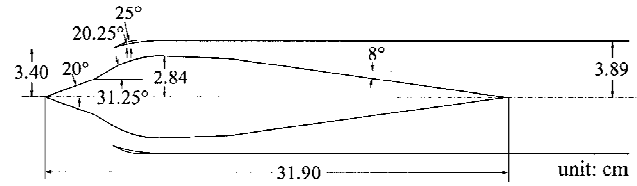


**Fig. 5 Supersonic inlet with mixed compression.**

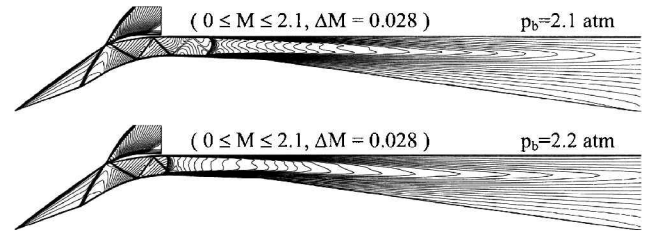


**Fig. 6 Mach number contours with different back pressures under steady-state conditions.**

The situation is much more complicated in a supersonic PDE due to the shock-wave/boundary-layer interaction and shock/acoustic-wave interaction[51] [also Oh, J. Y., Ma, F. H., Hsieh, S. Y., and Yang, V., "Interactions Between Shock Waves and Acoustic Waves in a Supersonic Inlet Diffuser" (to be submitted for publication)]. The engine dynamics exhibits features that are qualitatively different from those predicted by treating the inlet and combustor as two separate entities.

The inlet analysis is based on the axisymmetric, Favre-averaged conservation equations. Turbulence closure is achieved using a two-layer model of Rodi calibrated for supersonic flows with shock waves.[52] The governing equations are solved numerically by means of a density-based, finite volume methodology. The temporal discretization is obtained using a four-stage Runge–Kutta integration method, and the spatial discretization employs an upwind total-variation-diminishing scheme developed by Harten[53] Specific details of the numerical algorithm can be found in Ref. 54.

Figure 5 shows the configuration treated in the present study, a mixed-compression inlet optimized for a flight altitude of 9.3 km and a freestream Mach number of 2.1 (Ref. 50). Figure 6 presents the Mach-number contours at two different back pressures ($p_b = 2.1$ and 2.2 atm), which are carefully chosen such that the engine operates at a supercritical condition to provide a sufficient shock stability margin. Under these conditions, the two leading conical shocks generated by the double-cone centerbody compress the airflow externally, merge slightly above the cowl lip, and form a strong oblique shock, which extends into the external-flow region. In addition, a shock stemming from the cowl inner surface continues downstream, hitting and reflecting from both the cowl and centerbody walls, and finally leading to a terminal normal shock. The flow undergoes a sequence of compression and expansion waves and becomes subsonic after passing through the normal shock located in the divergent section of the diffuser. The inlet recovers a high percentage of the freestream total pressure by decelerating the airflow through the shock train. The pressure recovery coefficients for the two cases are 84 and 88%, respectively, and the Mach numbers immediately in front of the terminal shocks are 1.42 and 1.32, respectively.

The response of the inlet shock system to downstream disturbances has also been studied by imposing periodic pressure oscillations at the exit plane. A wide range of fluctuation frequency and amplitude were considered. Important phenomena of concern include temporal and spatial variations of mass flow rate, pressure recovery, and flow distribution, as well as shock displacement. In general, the acoustic response of the inlet flow increases with increasing amplitude of the imposed oscillation, but decreases with frequency. Also included as part of the result is the acoustic impedance function at the inlet exit, a parameter that can be effectively used to characterize the inlet/combustor coupling. A more detailed discussion on this subject will be given in subsequent work.

### B. Detonation Chamber Dynamics

The detonation chamber dynamics is formulated based on the conservation laws for a multicomponent chemically reacting system in two-dimensional coordinates. Diffusive transport is neglected in the current study because of its minor role in determining detonation dynamics and system performance. The governing equations and their associated boundary conditions are solved using a recently developed space–time conservation-element/solution-element method that circumvents the deficiencies of existing numerical methods for treating detonation waves and shock discontinuities.[55–59] The resultant computer code is further parallelized using the message passing interface library with domain decomposition to improve its efficiency.

Both simple global and detailed chemical kinetics models are utilized.[49,59] The former involves only one progress variable to characterize the chemical reaction rate and assumes constant properties. Because of its computational efficiency and reasonable accuracy in determining the PDE propulsive performance, the model is implemented in the present work. The associated thermochemical parameters are optimized by comparing the calculated detonation wave properties with those from the NASA chemical equilibrium analysis.[48] The relative errors are less than 5% in terms of the detonation velocity and the C–J pressure and temperature.

As part of the model validation effort, a series of single-pulse calculations were conducted for a straight tube of 60 cm in length initially filled with a stoichiometric mixture of hydrogen and air at preconditioned pressure $p_i$ and temperature $T_i$. A driver-gas region spanning 0.2 mm near the head end with a temperature of 2000 K and a pressure of 30 atm was employed to initiate the detonation wave directly. Four different numerical grids, with the sizes of 0.2, 0.1, 0.05, and 0.025 mm, were used to check the solution accuracy in terms of grid independence. All of the calculated pressure profiles collapsed onto a single curve, with the C–J properties matching the analytical values exactly. As a result, the 0.2-mm grid was chosen for the entire study to alleviate the computational burden. For a single-pulse operation, the head-end pressure remains at a plateau value $p_p$, that is, $p_3$ in Refs. 37 and 46, for certain period soon after the detonation initiation and then decays gradually to a level lower than the ambient state.[37,46] The impulse can be determined by integrating temporally the force exerted on the head end from $t = 0$ to the instant when the head-end pressure reaches the ambient value. The contribution to the impulse from the ignition source is estimated to be less than 0.5%. Figure 7 shows the impulse per unit cross-sectional area as a function of the plateau pressure $p_p$ and the detonation residence time $\tau_D$ (defined as the tube length $L$ divided by the detonation wave velocity $u_D$, i.e., $\tau_D \equiv L/u_D$). Results can be correlated well in the following form:

$$I/A = 4.1(p_p - p_i)\tau_D \tag{8}$$

This expression is quite similar to those obtained from the semi-analytical analysis of Wintenberger et al.[37] and the experimental work of Falempin et al.[14] The constants of proportionality differ slightly in the various studies, for example, 4.13 in Ref. 37 for the current conditions, suggesting dependence on the details of experimental procedure and operating conditions. The generalized formula proposed by Kailasanath[60] based on his numerical simulations for hydrogen/air, ethylene/oxygen, and propane/oxygen mixtures has a larger constant of proportionality of 4.65. One factor contributing to this disparity may be differences in ignition source. The width of the detonation initiation region is 20 mm in Ref. 60, as opposed to 0.2 mm in the present simulations. Nonetheless, the preceding parametric study demonstrates the capacity and fidelity of the present approach for the PDE performance analysis.

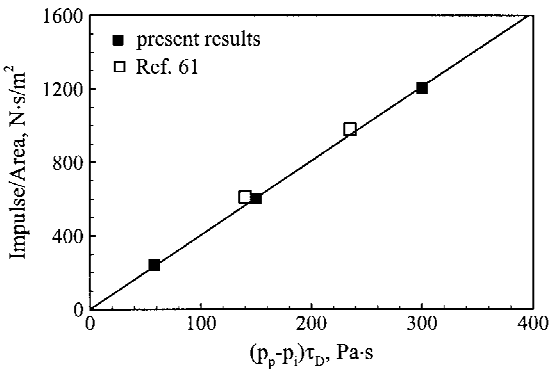


**Fig. 7 Generalized impulse curve for single-pulse detonation in straight tube with stoichiometric $H_2$/air mixture.**

The validated analysis is then employed to study the performance of airbreathing PDEs. As a specific example, the flight condition involving an altitude of 9.3 km and a Mach number of 2.1 is considered. The freestream static pressure and temperature are 0.29 atm and 228 K, respectively, corresponding to a total pressure of 2.65 atm and a total temperature of 428 K. The total pressure and temperature at the combustor entrance, obtained from the inlet flow analysis described in the preceding section, are 2.12 atm and 428 K, respectively. The detonation tube is 60 cm long and has a diameter of 16 cm, which is similar to the dimensions of contemporary ramjet combustors for air defense applications. As a first approach, only a single straight tube is considered to provide direct insight into the chamber dynamics without complications arising from the nozzle. The interactions among the tubes are also ignored. The valve at the tube entrance is assumed to be either fully open or fully closed. The operation sequence is, thus, controlled by three time periods: the valve close-up period, $\tau_{close}$, during which the valve is closed and the tube undergoes detonation initiation and propagation and blowdown processes; the purging period, $\tau_{purge}$, during which a small amount of cold air is injected to prevent preignition of fresh reactants; and the refilling period, $\tau_{refill}$, during which the combustible mixture is delivered to the chamber. The sum of these three periods is equal to the operation cycle period, $\tau_{cycle}$, that is, $\tau_{cycle} = \tau_{close} + \tau_{purge} + \tau_{refill}$. The purging period should be minimized to reduce performance loss. A small value of 0.1 ms is used throughout all of the calculations in the present study.

The boundary conditions at the head end of the detonation tube are specified according to the engine operation. During the purging and refilling stages, the total pressure and total temperature are obtained from the inlet analysis. The axial velocity is extrapolated from the interior points, and the reactant mass fraction is treated as an input parameter. When the valve is closed, the head end is simply modeled as a rigid wall.

A series of analyses are conducted over a wide range of operation parameters. The baseline case has $\tau_{cycle}$ of 3 ms and $\tau_{close}$ of 2.4 ms. The tube is initially filled with a stoichiometric hydrogen/air mixture at ambient pressure and temperature. It takes about five cycles to reach steady cyclic operation. Figure 8 shows the $x$–$t$ diagram for the first cycle of operation, obtained by tracing the characteristic lines of the flowfield along the centerline of the tube. The time histories of the flow properties at the head end are also presented. The detonation wave is directly initiated by a hot driver gas and propagates downstream at the C–J velocity toward the unburned mixture (region 1). It then induces Taylor expansion waves (region 2) to satisfy the stationary condition at the head end, causing a uniform region (region 3) with constant-flow properties in the upstream.

The detonation wave reaches the reactant/air interface at the tube exit at $t = 0.305$ ms (point A), which deviates slightly from the following analytical prediction by 0.6% due to the effect of the externally imposed ignition source:

$$\tau_D = L/u_D = 0.6\ \text{m}/1956\ \text{m/s} = 0.307\ \text{ms} \tag{9}$$

The wave then degenerates to a nonreactive shock, that is, the primary shock wave, proceeding farther downstream into the external region, followed by a contact surface separating the ambient air and combustion products. A sonic region is gradually formed near the tube exit due to the local flow expansion, as evidenced by the clustered characteristic lines in the $x$–$t$ diagram. Downstream of the sonic region, the flow is expanded to become supersonic and finally leads to the formation of a secondary shock to match with the subsonic flow behind the primary shock. This secondary shock wave

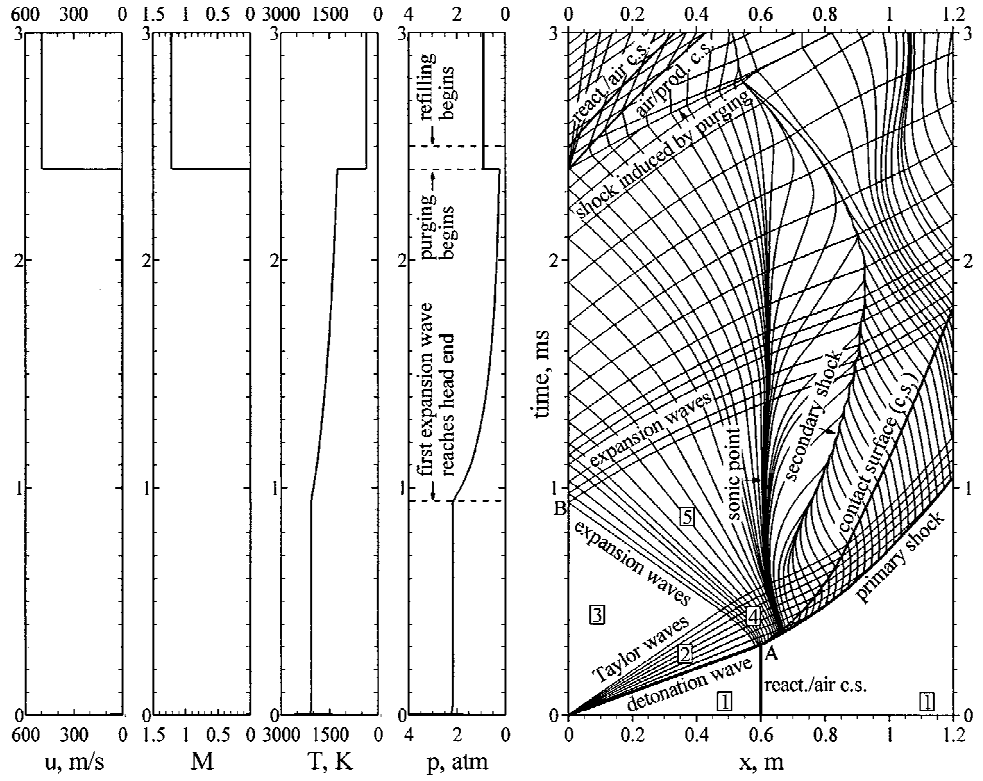


**Fig. 8 First cycle $x$–$t$ diagram and time histories of flow properties at head end under typical PDE operation: stoichiometric $H_2$/air mixture, $\tau_{cycle} = 3$ ms, $\tau_{close} = 2.4$ ms, and $\tau_{purge} = 0.1$ ms; 1 = unburned region, 2 = Taylor expansion waves, 3 = stationary region, 4 = non-simple wave region, and 5 = simple wave region.**

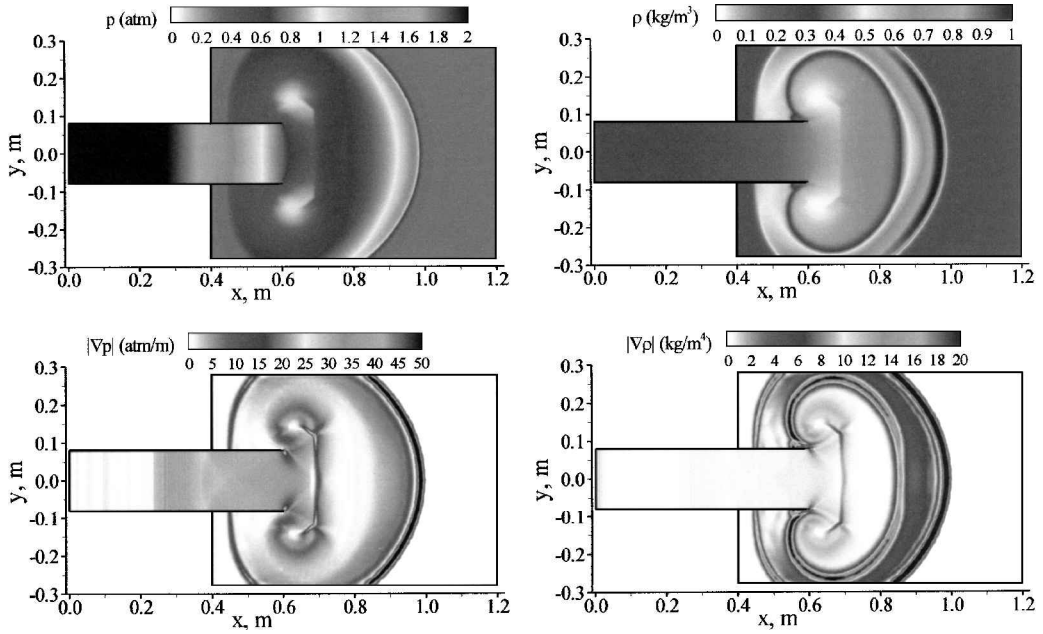


**Fig. 9 Snapshots of pressure, density and their gradients fields at $t = 0.7$ ms.**

moves farther downstream, meeting with expansion waves originating from the primary shock wave. These complicated flow structures can be also observed in Fig. 9, which shows the instantaneous pressure and density and their gradient fields at $t = 0.7$ ms. Many salient features are clearly shown, including the expansion fans, vortices, and rolled-up slip lines that are developed as the shock diffracts over the edge of the tube exit.

As the detonation wave catches the reactant/air interface and the resultant primary shock wave travels outside the tube, a series of expansion waves is generated, which propagate upstream, resulting in a nonsimple wave region (region 4) when interacting with the incoming Taylor waves. A simple wave region (region 5) is recovered after passing through the Taylor waves. The first expansion wave reaches the head end at $t = 0.935$ ms (point B), which can be determined by considering the interaction between the expansion and the Taylor waves and the sound speed in region 3. A similarity solution has been derived by Wintenberger et al.[37] to predict this time instant analytically,

$$t = L/u_D + \alpha(L/c_3) \tag{10}$$

where $\alpha$ is function of $\gamma$ and $M_D$ and can be calculated as

$$\alpha = \frac{1}{2}\left(1+\frac{1}{M_D^2}\right)\cdot\left\{2\left[\frac{\gamma-1}{\gamma+1}\left(\frac{\gamma+3}{2}+\frac{2}{\gamma-1}-\frac{(\gamma+1)^2}{2}\cdot\frac{M_D^2}{1+\gamma M_D^2}\right)\right]^{-(\gamma+1)/2(\gamma-1)}-1\right\} \tag{11}$$

Application of Eqs. (10) and (11) gives rise to an analytical value of 0.958 ms. The slight difference between the numerical and the analytical solutions may be attributed to the numerical resolution and dissipation near the tube exit.

On the arrival of the first expansion wave at the head end, the pressure begins to decay gradually. These expansion waves reflect off the head end and form another series of expansion waves, further reducing the chamber pressure. The downstream-traveling expansion waves weaken the secondary shock and eventually cause it to move upstream.

The head-end pressure decays to 0.23 atm at $t = 2.4$ ms, at which point the purging stage begins. The head-end temperature is 1258 K at this instant. Because of the pressure difference across the entrance plane, a right-running shock wave is established, along with a series of central expansion waves and a contact surface between the burned gas and the cold air. Another contact surface forms between the fresh reactants and purging air when the refilling stage commences 0.1 ms later. The corresponding refilling pressure, velocity, and Mach number are about 0.91 atm, 500 m/s, and 1.2, respectively. The time evolution of the pressure distribution along the centerline during the first cycle of operation is shown in Fig. 10.

The flow evolution during a steady operation cycle is examined. Figure 11 shows the $x$–$t$ diagram and time histories of flow properties at the head end for the fifth cycle. The main flow features remain qualitatively the same as those in the first cycle. However, the secondary shock wave disappears because the flow behind the primary shock wave is already supersonic. In addition, the head-end pressure and temperature begin to decay earlier relative to the first cycle, due to the rarefaction waves produced from the previous cycle. Also note that the detonation wave catches the leading fresh reactant at $x = 51.2$ cm instead of at the tube exit.

The impulse of each cycle is calculated by considering the momentum balance over a control volume enclosing the entire engine. The inlet flow loss is properly taken into account as detailed in Sec. III.A. The cycle-averaged specific thrust (air based) and specific impulse (fuel based) are then obtained by dividing the impulse by the air mass and fuel weight for each cycle, respectively. For the baseline case, the fuel-based specific impulse is 2328 s. This may be compared to a ramjet engine operating at the same flight condition with perfect nozzle flow expansion, which has a specific impulse of about 3866 s (Ref. 61). A parametric study was carried out to examine the effect of various operating times on the system performance. Figure 12 shows the result as a function of $\tau_{\text{close}}$. The straight-tube system leads to a specific impulse far lower than its theoretical limit of 5263 s based on the thermodynamic cycle analysis for an ideal PDE, Eq. (7), which assumes isentropic flow processes in the inlet and nozzle. Although the calculated specific impulse can be improved by optimizing the operation frequency and timing, the net gain appears to be limited with the current design. Several fundamental mechanisms responsible for such an unacceptable performance have been identified. First, at high altitudes, the straight-tube design fails to preserve the chamber pressure during the refilling stage at a level sufficient to meet the requirements for the mass loading density of fresh reactants. Second, the low chamber pressure in the refilling stages causes a high-speed reactant stream in the tube and, subsequently, results in a large performance loss. It is well established that the stagnation pressure drop due to energy addition is proportional to the square of the Mach number. In the present case, the local Mach number may reach a value of up to 1.2 during the refilling process. The ensuing loss of thermodynamic efficiency becomes exceedingly large compared with conventional propulsion systems with subsonic combustion. Third, the lack of

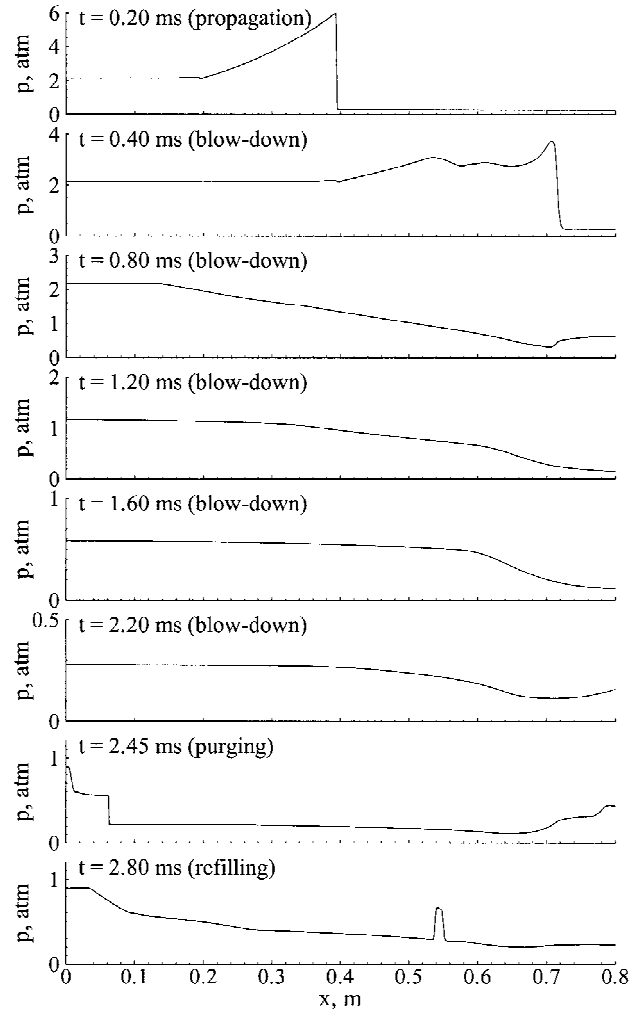


**Fig. 10 Time evolution of pressure distribution along centerline during first cycle of operation: $\tau_{\text{cycle}} = 3$ ms, $\tau_{\text{close}} = 2.4$ ms, and $\tau_{\text{purge}} = 0.1$ ms.**

an appropriate flow expansion device downstream of the detonation tube gives rise to an extremely complicated flow structure near the tube exit. The internal energy of the exhaust flow can not be effectively converted to the kinetic energy for thrust generation, further deteriorating the situation.

### C. Effect of Nozzle Configuration

In light of the limited performance of the straight-tube design, much effort was expended to study the effect of nozzle configuration on the system propulsive performance. The nozzle design for PDEs poses a serious challenge because of the intrinsically unsteady nature of the pulse detonation process. Recent studies based on single-pulse calculations[41,42] and experiments[12,21,62] indicate that the nozzle configuration may significantly change the thrust delivered by an engine. In addition to its influence on specific impulse through modification of the gas expansion process, the nozzle affects the chamber flow dynamics and, consequently, the timing of various phases of the engine operation cycle, especially for high-altitude and space applications.

The present work focuses on a choked convergent–divergent (C–D) nozzle because of its effectiveness in preserving the chamber pressure during the blowdown and refilling stages. In contrast, divergent and plug nozzles do not possess such an advantage, especially under high-altitude conditions, in spite of their superior performance for single-pulse operation at sea level. Figure 13 shows schematically the nozzle configuration considered herein, measuring a length of 20 cm. The slope angle is 45 deg for the convergent part and 15 deg for the divergent part. The ratio of the tube

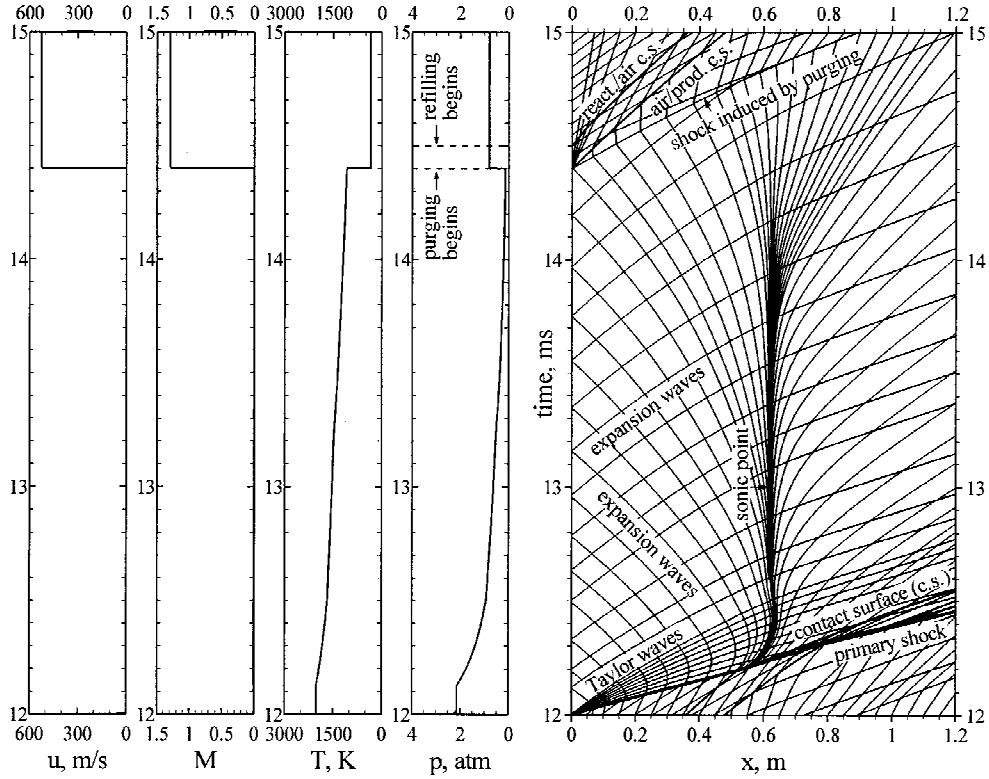


**Fig. 11 Fifth cycle $x$–$t$ diagram and time histories of flow properties at head end under typical PDE operation: stoichiometric $H_2$/air mixture, $\tau_{cycle} = 3$ ms, $\tau_{close} = 2.4$ ms, and $\tau_{purge} = 0.1$ ms.**

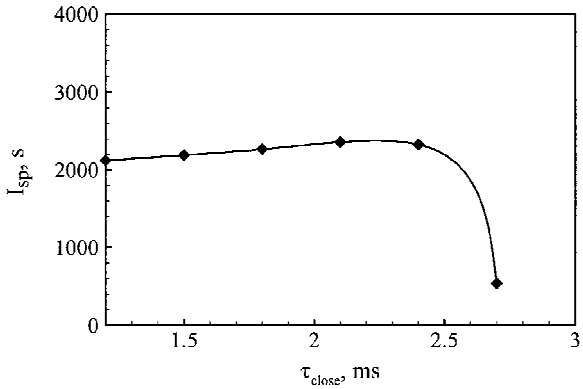


**Fig. 12 Effect of valve close-up time on specific impulse, $\tau_{cycle} = 3$ ms and $\tau_{purge} = 0.1$ ms; straight tube with stoichiometric $H_2$/air mixture, $h = 9.3$ km, and $M_\infty = 2.1$.**

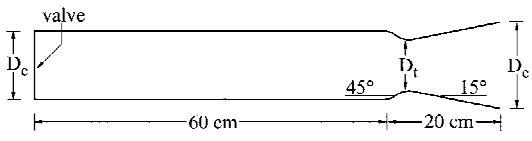


**Fig. 13 Configuration of single-tube PDE with C–D nozzle.**

cross-sectional area to the nozzle throat area is 1.78, and the nozzle expansion ratio is 2.81. Several calculations were conducted for this configuration. The baseline case has $\tau_{cycle}$ of 3 ms and $\tau_{close}$ of 2.1 ms. The detonation tube is initially filled with a stoichiometric hydrogen/air mixture and the nozzle with air. The engine takes five cycles to reach steady operation. Figures 14 and 15 show the $x$–$t$ diagrams along the centerline of the tube and the time histories of flow properties at the head end for the first and eighth cycles of operation, respectively. The flow characteristics bear close resemblance to those of the straight-tube case. A major difference lies in the reflection of a shock wave from the convergent section of the nozzle, instead of expansion waves in a straight tube. The reflected shock then propagates upstream and causes an abrupt increase in pressure at the head end on its arrival, as evidenced in the pressure–time trace in Fig. 14. The nozzle throat remains choked during most of the cycle, thus helping preserve the chamber pressure. The pressure in the refilling stage is about 1.45 atm, which is substantially greater than the straight-tube case and, consequently, increases the mass loading density of fresh reactants. The relatively lower speed of the refilled mixture also enhances the system thermodynamic efficiency. The specific impulse of 3402 s in the present case is 46% higher than the maximum specific impulse achieved by a straight tube, further demonstrating the effectiveness of a choked C–D nozzle in improving engine performance.

A parametric study is conducted to study the timing effect on system performance by varying $\tau_{cycle}$ and $\tau_{close}$. The purge time $\tau_{purge}$ is fixed at 0.1 ms. Figure 16 shows the effect of $\tau_{close}$ on the specific thrust $F_{sp}$, defined as the cycle-averaged thrust per unit of air mass flow rate, and the fuel-based specific impulse $I_{sp}$ at four different cycle frequencies of 200, 250, 333, and 400 Hz. The corresponding cycle periods are 5, 4, 3, and 2.5 ms, respectively. When the straight-tube design is compared at the same operating condition, the present system with a choked C–D nozzle can indeed substantially improve the engine performance by a margin of 45%.

The specific thrust increases as $\tau_{close}$ decreases for all of the frequencies considered herein. This can be explained as follows. For a given $\tau_{cycle}$ and $\tau_{purge}$, a smaller $\tau_{close}$ translates to a shorter blowdown process. The resultant higher chamber pressure during the refilling stage increases the loading density of fresh reactants. The increased refilling period also enhances the amount of reactants delivered to the chamber. Combined, these two factors result in a higher cycle-averaged chamber pressure and, consequently, a higher specific thrust. Note, however, that the lower bound of $\tau_{close}$ is subject to three practical constraints. The first is concerned with inlet overpressurization. The head-end pressure must not exceed the stagnation pressure of the inlet air to allow for purging and refilling when the valve is open. The second is related to chamber overfilling. The fresh reactants should not flow out of the nozzle to the external region before being burned completely unless afterburning is considered.

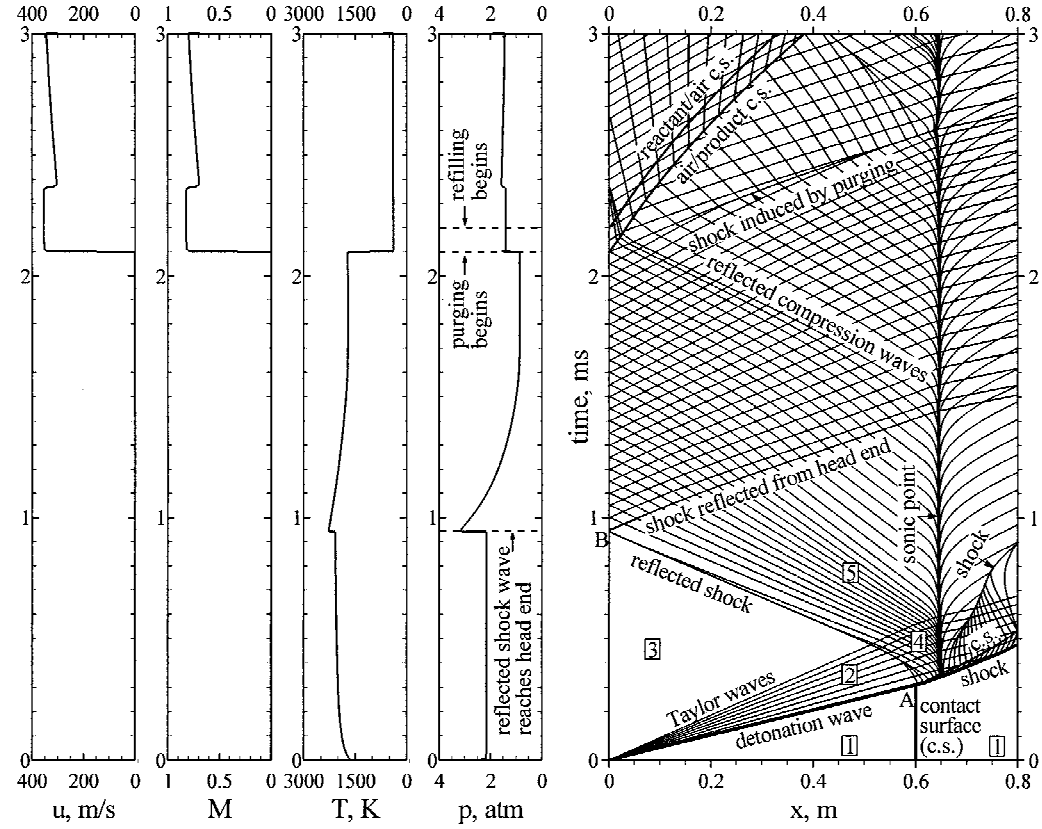


**Fig. 14 First cycle *x–t* diagram and time histories of flow properties at head end under typical PDE operation with C–D nozzle: stoichiometric $H_2$/air mixture, $\tau_{cycle} = 3$ ms, $\tau_{close} = 2.1$ ms, and $\tau_{purge} = 0.1$ ms; 1 = uniform unburned region, 2 = Taylor expansion waves, 3 = uniform region, 4 = non-simple wave region, and 5 = simple wave region.**

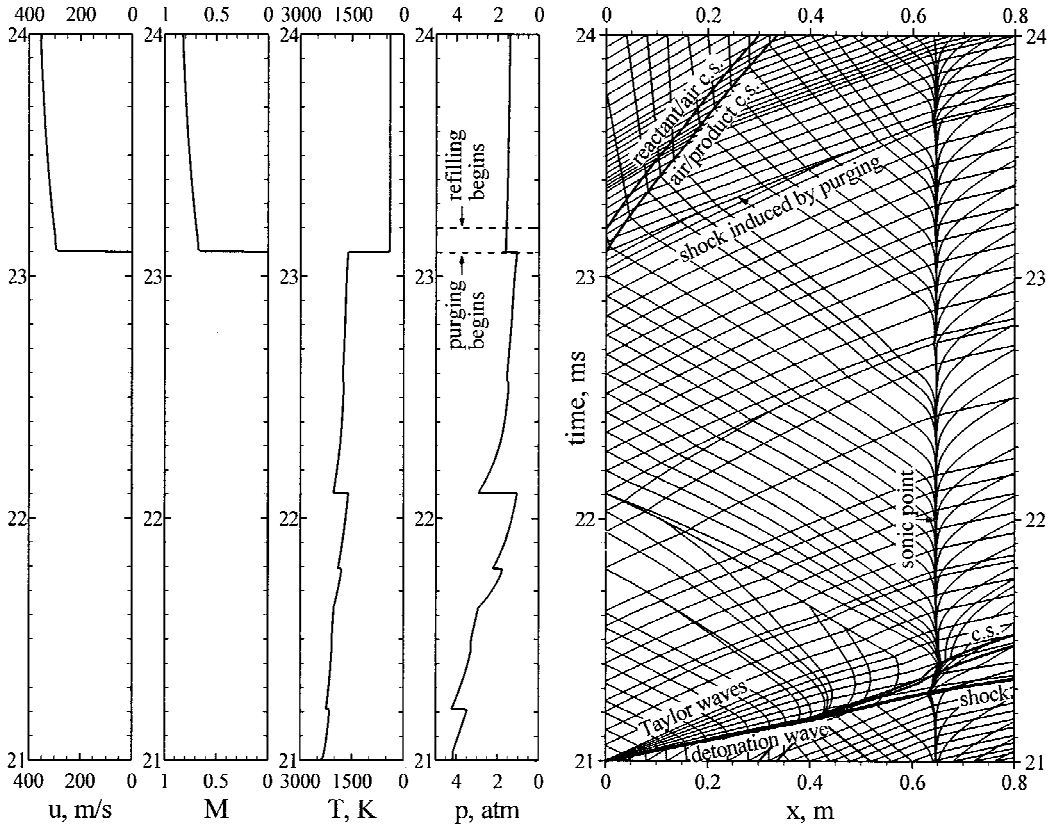


**Fig. 15 Eighth cycle *x–t* diagram and time histories of flow properties at head end under typical PDE operation with C–D nozzle: stoichiometric $H_2$/air mixture, $\tau_{cycle} = 3$ ms, $\tau_{close} = 2.1$ ms, and $\tau_{purge} = 0.1$ ms.**

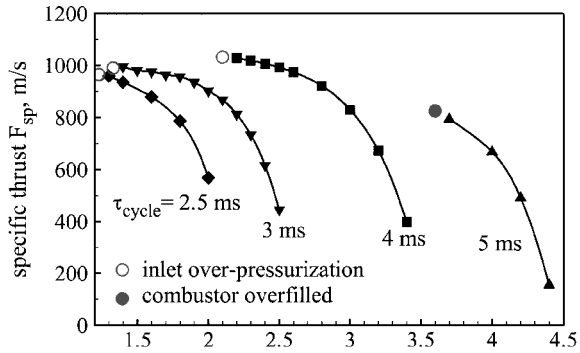


**a) Air-based specific thrust**

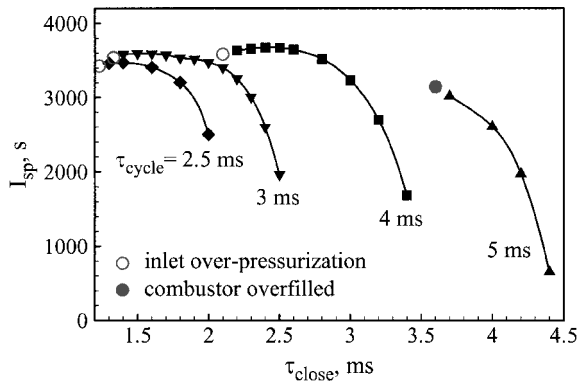


**b) Fuel-based specific impulse**

**Fig. 16 Effect of valve close-up time at four different operation frequencies, straight tube with C–D nozzle for stoichiometric $H_2$/air mixture, $h = 9.3$ km, $M_\infty = 2.1$.**

The third constraint, although commonly satisfied in practical cases, is that $\tau_{close}$ should be sufficiently long to cover at least the time required for detonation initiation and propagation throughout the entire chamber. The upper bound of $\tau_{close}$ (or the lower bound of $\tau_{refill}$) is based on the requirement that an appropriate amount of fresh reactants be delivered to the chamber to produce thrust.

The effect of $\tau_{close}$ on the fuel-based specific impulse follows the same trend as that of the air-based specific thrust, except for a small range of $\tau_{close}$ close to its lower bound. The specific impulse and specific thrust satisfy the following relation:

$$I_{sp} = \frac{F_{sp}(1 + \tau_{purge}/\tau_{refill})}{fg} \tag{12}$$

As $\tau_{close}$ decreases, the factor $(1 + \tau_{purge}/\tau_{refill})$ decreases and may override the increase of $F_{sp}$, consequently leading to a decrease in $I_{sp}$, as shown in Fig. 16b.

For a given cycle period, $\tau_{close}$ determines the filling length of fresh reactants. A larger $\tau_{close}$ (or smaller $\tau_{refill}$) leads to a smaller filling length in most cases and, consequently, decreases the specific impulse. This result, however, is in contrast to the previous experimental[62] and numerical[47] observations for single-pulse operations, which concluded that the specific impulse increases as the filling length decreases. One factor contributing to this discrepancy is that, in single-pulse studies, the pressure and temperature of reactants are preconditioned to ambient values, whereas in the present multicycle study the flow conditions of the refilled mixture depend on the timing of the engine operation. The use of a choked C–D nozzle also exerted a substantial influence on the chamber dynamics. Thus, significant differences exist between single-pulse and multicycle operations. The conclusions from single-pulse studies may not be applied to multicycle cases directly.

Figure 16 also demonstrates the existence of an optimum frequency for achieving a maximum performance for a given PDE configuration and flight condition. At a low cycle frequency, more reactants can be recharged into the detonation tube. As a consequence, a higher chamber pressure can be reached, and the engine efficiency improves. However, a large refilling time associated with low-frequency operation may cause chamber overfilling and, thus, degrade the performance. These two conflicting effects result in an optimum frequency. In the present study, the operating frequency of 250 Hz ($\tau_{cycle} = 4$ ms) offers the best performance. The highest specific impulse is 3676 s, slightly lower than its ramjet counterpart of 3866 s with optimum nozzle flow expansion.

## IV. Conclusions

A comprehensive analysis has been established to study the system performance of airbreathing PDEs. The physical model of concern includes inlet, air-distribution unit, detonation tube, and nozzle. Results from parametric studies reveal that, for a fixed operating frequency, a decrease in $\tau_{close}$ leads to increased engine performance in terms of specific impulse and thrust. The straight-tube design gives rise to unacceptable performance, especially for high-altitude applications, due to its failure to preserve chamber pressure during the refilling stage. A choked C–D nozzle appears to be required to deliver performance at a level sufficient to compete with other airbreathing engines, such as ramjets. For a given engine configuration and flight condition, an optimum cycle frequency and $\tau_{close}$ exist for achieving the best performance. A thermodynamic cycle analysis was also developed to determine the theoretical limit of the engine propulsive efficiency. Results were compared with those of the Humphrey and Brayton cycles.

For a typical supersonic mission with a flight Mach number of 2.1 and an altitude of 9.3 km, the maximum PDE specific impulse is 3676 s for a stoichiometric hydrogen/air mixture with proper account of the inlet and nozzle performance losses. This $I_{sp}$ is lower than its ramjet counterpart of 3866 s with perfect nozzle flow expansion. Furthermore, the intrinsic unsteadiness, thrust vector variation, and other loss mechanisms not considered in the present analysis (such as the energy required for detonation initiation and flow losses associated with the inlet isolator, rotary valve, and air distributor) may render the PDE much less attractive. Further improvement and optimization of the system configuration and operation are required.

## Acknowledgments

This work was supported by the Department of Defense Multidisciplinary University Research Initiative under the Office of Naval Research Grant N00014-99-1-0744, with Gabriel Roy serving as the Program Manager.

## References

[1]Bussing, T. R. A., and Pappas, G., "Pulse Detonation Engine Theory and Concepts," *Developments in High-Speed Vehicle Propulsion Systems*, Vol. 165, Progress in Astronautics and Aeronautics, AIAA, Reston, VA, 1996, pp. 421–472.

[2]Hoffman, N., "Reaction Propulsion by Intermittent Detonative Combustion," Ministry of Supply, Volkenrode Translation, 1940.

[3]Nicholls, J. A., Wilkinson, H. R., and Morrison, R. B., "Intermittent Detonation as a Thrust-Producing Mechanism," *Jet Propulsion*, Vol. 27, No. 5, 1957, pp. 534–541.

[4]Krzycki, L. J., "Performance Characteristics of an Intermittent-Detonation Device," U.S. Naval Ordnance Test Station, NAVWEPS Rept. 7655, China Lake, CA, 1962.

[5]Helman, D., Shreeve, R. P., and Eidelman, S., "Detonation Pulse Engine," AIAA Paper 86-1683, June 1986.

[6]Hinkey, J. B., Bussing, T. R. A., and Kays, L., "Shock Tube Experiments for the Development of a Hydrogen-Fueled Pulse Detonation Engine," AIAA Paper 95-2578, July 1995.

[7]Sterling, J., Ghorbanian, K., Humphrey, J., and Sobota, T., "Enhanced Combustion Pulsejet Engines for Mach 0 to 3 Applications," AIAA Paper 96-2687, July 1996.

[8]Litchford, R. J., "Development of a Gas-Fed Pulse Detonation Research Engine," AIAA Paper 2001-3814, July 2001.

[9]Shepherd, J. E., Pintgen, F., Austin, J. M., and Eckett, C. A., "The Structure of the Detonation Front in Gases," AIAA Paper 2002-0773, Jan. 2002.

[10]Meyer, T. R., Hoke, J. L., Brown, M. S., Gord, J. R., and Schauer, F. R., "Experimental Study of Deflagration Enhancement Techniques in a H2/Air Pulsed-Detonation Engine," AIAA Paper 2002-3720, July 2002.

[11]Sanders, S. T., Jenkins, T. P., and Hanson, R. K., "Diode Laser Sensor System for Multi-Parameter Measurements in Pulse Detonation Engine Flows," AIAA Paper 2000-3593, July 2000.

[12]Daniau, D., Zitoun, R., Couguet, C., and Desbordes, D., "Effects of Nozzles of Different Length and Shape on the Propulsion Performance of Pulsed Detonation Engines," High Speed Deflagration and Detonation, Fundamentals and Control, edited by G. Roy, S. Frolov, D. Netzer, and A. Borisov, ELEX-KM Publishers, Moscow, 2001, pp. 251–262.

[13]Sinibaldi, J. O., Brophy, C. M., Li, C., and Kailasanath, K., "Initiator Detonation Diffraction Studies in Pulsed Detonation Engines," AIAA Paper 2001-3466, July 2001.

[14]Falempin, F., Bouchaud, D., Forrat, B., Desbordes, D., and Daniau, E., "Pulsed Detonation Engine: Possible Application to Low Cost Tactical Missile and to Space Launcher," AIAA Paper 2001-3815, July 2001.

[15]Broda, J. C., Conrad, C., Pal, S., Woodward, R. D., and Santoro, R. J., "Experimental Results on Air-Breathing Pulse Detonation Studies," *Proceedings of 11th Annual Symposium on Propulsion*, 1999.

[16]Watts, J., Conrad, C., Lee, S. Y., Woodward, R. D., Pal, S., Santoro, R. J., "Fundamental Studies of the DDT Process in Pulse Detonation Engines Based on Single/Multi-Cycle Operation," *Proceedings of 12th Annual Symposium on Propulsion*, 2000.

[17]Sinibaldi, J. O., Brophy, C. M., and Robinson, L. J. P., "Ignition Effects on Deflagration-to-Detonation Transition Distance in Gaseous Mixtures," AIAA Paper 2000-3590, July 2000.

[18]Cooper, M, Jackson, S., Austin, J., Wintenberger, E., and Shepherd, J. E., "Direct Experimental Impulse Measurements for Detonations and Deflagrations," *Journal of Propulsion and Power*, Vol. 18, No. 5, 2002, pp. 1033–1041.

[19]Harris, P. G., Farinaccio, R., and Stowe, R. A., "The Effect of DDT Distance on Impulse in a Detonation Tube," AIAA Paper 2001-3467, July 2001.

[20]Lieberman, D. H., Parkin, K. L., and Shepherd, J. E., "Detonation Initiation by a Hot Turbulent Jet for Use in Pulse Detonation Engines," AIAA Paper 2002-3909, July 2002.

[21]Stuessy, W. S., and Wilson, D. R., "Experimental Investigation of an Annual Multi-Cycle Pulsed Detonation Wave Engine," AIAA Paper 96-0346, Jan. 1996.

[22]Aarnio, M. J., Hinkey, J. B., and Bussing, T. R. A., "Multiple Cycle Detonation Experiments during the Development of a Pulse Detonation Engine," AIAA Paper 96-3263, July 1996.

[23]Hinkey, J. B., Williams, J. T., Henderson, S. E., and Bussing, T. R. A., "Rotary-Valved, Multiple-Cycle, Pulse Detonation Engine Experimental Demonstration," AIAA Paper 97-2746, 1997.

[24]Schauer, F., Stutrud, J., and Bradley, R., "AFRL's In-House Research Pulse Detonation Engine," *Proceedings of 11th Annual Symposium on Propulsion*, 1999.

[25]Schauer, F., Stutrud, J., Bradley, R., and Katta, V., "AFRL/PRSC Pulse Detonation Engine Research Program," *Proceedings of 12th Annual Symposium on Propulsion*, 2000.

[26]McManus, K., Furlong, E., Leyva, I., and Sanderson, S., "MEMS-Based Pulse Detonation Engine for Small-Scale Propulsion Applications," AIAA Paper 2001-3469, July 2001.

[27]Frankey, B., Shauer, F., Bradley, R., and Hoke, J., "Evaluation of a Hybrid-Piston Pulsed Detonation Engine," AIAA Paper 2002-0474, Jan. 2002.

[28]Brophy, C. M., Sinibaldi, J. O., and Damphousse, P., "Initiator Performance for Liquid-Fueled Pulse Detonation Engines," AIAA Paper 2002-0472, Jan. 2002.

[29]Shimo, M., Meyer, S. E., Heister, S. D., Weng, C. S., Ji, J., and Gore, J. P., "An Experimental and Computational Study of Pulsed Detonations in a Single Tube," AIAA Paper 2002-3716, July 2002.

[30]Brophy, C. M., Netzer, D. W., and Forster, L. D., "Detonation Studies of JP-10 with Oxygen and Air for Pulse Detonation Engine Development," AIAA Paper 98-4003, July 1998.

[31]Brophy, C. M., and Netzer, D. W., "Effects of Ignition Characteristics and Geometry on the Performance of a JP-10/O2 Fueled Pulse Detonation Engine," AIAA Paper 99-2635, June 1999.

[32]Farinaccio, R., Harris, P., Stowe, R. A., and Akbar, R., "Multi-Pulse Detonation Experiments with Propane–Oxygen," AIAA Paper 2002-4070, July 2002.

[33]Talley, D. G., and Coy, E. B., "Constant Volume Limit of Pulsed Propulsion for a Constant $\gamma$ Ideal Gas," *Journal of Propulsion and Power*, Vol. 18, No. 2, 2002, pp. 400–406.

[34]Tew, D. E., "Ideal Polytropic Ramjet Performance," *Proceedings of 11th Annual Symposium on Propulsion*, 1999.

[35]Kentfield, J. A. C., "The Fundamentals of Idealized Airbreathing Pulse-Detonation Engines," *Journal of Propulsion and Power*, Vol. 18, No. 1, 2002, pp. 77–83.

[36]Heiser, W. H., and Pratt, D. T., "Thermodynamic Cycle Analysis of Pulse Detonation Engines," *Journal of Propulsion and Power*, Vol. 18, No. 1, 2002, pp. 68–76.

[37]Wintenberger, E., Austin, J. M., Cooper, M., Jackson, S., and Shepherd, J. E., "Analytical Model for the Impulse of a Single-Cycle Pulse Detonation Engine," *Journal of Propulsion and Power*, Vol. 19, No. 1, 2003, pp. 22–38.

[38]Sterling, J., Ghorbanian, K., Humphrey, J., and Sobota, T., "Numerical Investigations of Pulse Detonation Wave Engines," AIAA Paper 95-2479, July 1995.

[39]Mohanraj, R., and Merkle, C. L., "A Numerical Study of Pulse Detonation Engine Performance," AIAA Paper 2000-0315, Jan. 2000.

[40]Eidelman, S., Grossman, W., and Lottati, I., "Air-Breathing Pulsed Detonation Engine Concept; A Numerical Study," AIAA Paper 90-2420, July 1990.

[41]Eidelman, S., and Yang, X., "Analysis of the Pulse Detonation Engine Efficiency," AIAA Paper 98-3877, July 1998.

[42]Cambier, J. L., and Tegner, J. K., "Strategies for Pulsed Detonation Engine Performance Optimization," *Journal of Propulsion and Power*, Vol. 14, No. 4, 1998, pp. 489–498.

[43]Li, C., Kailasanath, K., and Patnaik, G., "A Numerical Study of Flow Field Evolution in a Pulsed Detonation Engine," AIAA Paper 2000-0314, Jan. 2000.

[44]Ebrahimi, H. B., Mohanraj, R., and Merkle, C.L., "Multilevel Analysis of Pulsed Detonation Engines," *Journal of Propulsion and Power*, Vol. 18, No. 2, 2002, pp. 225–232.

[45]Ebrahimi, H. B., Mohanraj, R., and Merkle, C. L., "Modeling of Multi-Tube Pulse Detonation Engine Operation," AIAA Paper 2001-3813, July 2001.

[46]Li, C., and Kailasanath, K., "A Numerical Study of Reactive Flows in Pulse Detonation Engines," AIAA Paper 2001-3933, July 2001.

[47]Li, C., and Kailasanath, K., "Performance Analysis of Pulse Detonation Engines with Partial Fuel Filling," AIAA Paper 2002-0610, Jan. 2002.

[48]McBride, B. J., and Gordon, S., "Computer Program for Calculation of Complex Chemical Equilibrium Compositions and Applications," NASA Reference Publ. 1311, June 1996.

[49]Wu, Y. H., "System Performance and Thermodynamic Cycle Analysis of Air-Breathing Pulse Detonation Engines," Ph.D. Dissertation, Dept. of Mechanical and Nuclear Engineering, Pennsylvania State Univ., University Park, PA, May 2002.

[50]Yang, V., and Cappuccio, M., "Supersonic Inlet Design for Missiles," Dept. of Mechanical Engineering, Research Rept., Pennsylvania State Univ., University Park, PA, 1990.

[51]Yang, V., and Culick, F. E. C., "Analysis of Unsteady Inviscid Diffuser Flow with a Shock Wave," *Journal of Propulsion and Power*, Vol. 1, 1985, pp. 222–228.

[52]Rodi, W., "Experience with Two-Layer Models Combining the $k$–$\varepsilon$ Model with a One-Equation Model Near the Wall," AIAA Paper 91-0216, Jan. 1991.

[53]Harten, A., "High Resolution Schemes for Hypersonic Conservation Laws," *Journal of Computational Physics*, Vol. 49, No. 3, 1983, pp. 357–393.

[54]Oh, J. Y., "Numerical Study of Steady and Oscillatory Flow Structures in an Axisymmetric Supersonic Inlet," Ph.D. Dissertation, Dept. of Mechanical Engineering, Pennsylvania State Univ., University Park, PA, Aug. 1994.

[55]Chang, S. C., "The Method of Space–Time Conservation Element and Solution Element—A New Approach for Solving the Navier–Stokes and Euler Equations," *Journal of Computational Physics*, Vol. 119, No. 2, 1995, pp. 295–324.

[56]Wang, X. Y., and Chang, S. C., "A 2D Non-Splitting Unstructured Triangular Mesh Euler Solver Based on the Space–Time Conservation Element and Solution Element Method," *Computational Fluid Dynamic Journal*, Vol. 8, No. 2, 1999, pp. 309–325.

[57]Chang, S. C., Wang, X. Y., and Chow, C. Y., "The Space–Time Conservation Element and Solution Element: A New High Resolution and Genuinely Multidimensional Paradigm for Solving Conservation Laws," *Journal of Computational Physics*, Vol. 156, No. 1, 1999, pp. 89–136.

[58]Zhang, Z. C., Yu, S. T., and Chang, S. C., "A Space–Time Conservation Element and Solution Element Method for Solving the Two- and Three-Dimensional Unsteady Euler Equations Using Quadrilateral and Hexahedral Meshes," *Journal of Computational Physics*, Vol. 175, No. 1, 2002, pp. 168–199.

[59]Wu, Y. H., Yang, V., and Chang, S. C., "Numerical Simulation of Chemically Reacting Flows with Detailed Kinetics Using the Space-Time Method," *Proceedings of 1st International Conference on Computational Fluid Dynamics*, Springer-Verlag, Berlin, 2000, pp. 207–212.

[60]Kailasanath, K., "Recent Developments in the Research on Pulse Detonation Engines," AIAA Paper 2002-0470, Jan. 2002.

[61]Yang, V., Ma, F. H., and Choi, J. Y., "System Performance and Thrust Chamber Optimization of Air-Breathing Pulse Detonation Engines," *Proceedings of 15th ONR Propulsion Meeting*, U.S. Naval Research Office, Washington, DC, 2002.

[62]Cooper, M., and Shepherd, J. E., "The Effect of Nozzles and Extensions on Detonation Tube Performance," AIAA Paper 2002-3628, July 2002.